

1 **The effect of local sources on particle size and chemical**  
2 **composition and their role in aerosol-cloud interactions**  
3 **at Puijo measurement station**

4  
5 **H. Portin<sup>1,2</sup>, A. Leskinen<sup>1</sup>, L. Hao<sup>2</sup>, A. Kortelainen<sup>2</sup>, P. Miettinen<sup>2</sup>, A.**  
6 **Jaatinen<sup>2</sup>, A. Laaksonen<sup>2,3</sup>, K. E. J. Lehtinen<sup>1,2</sup>, S. Romakkaniemi<sup>2</sup>, M.**  
7 **Komppula<sup>1</sup>**

8  
9 [1]{Finnish Meteorological Institute, P.O.Box 1627, FI-70211, Kuopio, Finland}

10 [2]{University of Eastern Finland, Department of Applied Physics, P.O.Box 1627, FI-  
11 70211, Kuopio, Finland}

12 [3]{Finnish Meteorological Institute, P.O.Box 503, FI-00101 Helsinki, Finland}

13  
14 Correspondence to: H. Portin (harri.portin@fmi.fi)

## 1 **Abstract**

2  
3 Interactions between aerosols and liquid water clouds were studied during autumns 2010-  
4 2011 at a semi-urban measurement station on Puijo tower in Kuopio, Finland. Cloud  
5 interstitial and total aerosol size distributions, particle chemical composition and  
6 hygroscopicity and cloud droplet size distribution were measured, with a focus on  
7 comparing clean air masses with those affected by local sources. On average, the polluted  
8 air contained more particles than the clean air masses and generally, the concentrations  
9 decreased during cloud events. The accumulation mode concentration in clean air was an  
10 exception, increasing by a factor of 2.4 during cloud events due to cloud processing. It  
11 was also observed for the polluted air but to a lesser extent. Some, mostly minor,  
12 differences in the average particle chemical composition between the air masses were  
13 observed. The average size and number concentration of activating particles were quite  
14 similar for both air masses, producing average droplet populations with only minor  
15 distinctions. As a case study, a long cloud event was analyzed in detail with a special  
16 focus on the emissions from local sources, including a paper mill and a heating plant.  
17 This revealed larger variations in particle and cloud properties than the analysis of the  
18 whole data set. Clear differences in the total (range 214...2200  $\text{cm}^{-3}$ ) and accumulation  
19 mode particle concentrations (62...169  $\text{cm}^{-3}$ ) were observed. Particle chemical  
20 composition, especially the concentrations of organics (0.42...1.28  $\mu\text{g m}^{-3}$ ) and  $\text{SO}_4$   
21 (0.16...4.43  $\mu\text{g m}^{-3}$ ) varied considerably. This affected the hygroscopic growth factor, e.g.  
22 for 100 nm particles the range was 1.21...1.45 at 90% relative humidity. Particularly,  
23 large particles, high hygroscopicities and elevated amounts of inorganics were linked  
24 with the pollutant plumes. Moreover, the particle hygroscopicity distributions in the  
25 polluted air were clearly bimodal, indicating externally mixed aerosol. The variable  
26 conditions also had an impact on cloud droplet formation, with the droplet concentration  
27 varying between 138...240  $\text{cm}^{-3}$  and mean diameter between 9.2...12.4  $\mu\text{m}$ .

## 1 **1 Introduction**

2  
3 Anthropogenic aerosol particles such as sulphates and carbonaceous aerosols have  
4 significantly increased the global mean burden of atmospheric aerosol compared to the  
5 pre-industrial times. Prediction of the current and future behaviour of the Earth's climate  
6 system is complicated by the large uncertainties associated with the indirect effects of  
7 atmospheric aerosols (Lohmann and Feichter, 2005, IPCC 2013).

8  
9 The indirect effect is characterized by the ability of aerosol particles to act as cloud  
10 condensation nuclei (CCN) or ice nuclei. More CCN means more and smaller droplets,  
11 which leads to the Twomey effect: higher cloud albedo and increased reflection of solar  
12 radiation (Twomey, 1977). Another consequence is the Albrecht effect: since droplets are  
13 smaller, the cloud liquid water path increases, precipitation development is weaker and  
14 the clouds are more persistent (Albrecht, 1989). However, this effect is more complicated  
15 than the Twomey effect, because, if cloud thermodynamics and dynamics are considered,  
16 the liquid water path may also decrease (Han et al., 2002).

17  
18 Particle size, number concentration and chemical composition are the key aerosol  
19 properties in the cloud droplet activation process (Dusek et al. 2006, Hudson, 2007),  
20 which has been confirmed in studies based on satellite observations (Brenquier et al.,  
21 2003, Sekiguchi et al., 2003), model calculations (Menon et al., 2002, Rotstayn and Liu,  
22 2005) and in-situ measurements (Coakley and Walsh, 2002, Wang et al., 2008). The  
23 effect of size and number concentration is well known (e.g. Vong and Covert, 1998,  
24 Henning et al., 2002, Komppula et al., 2005, Anttila et al., 2009), whereas the role of  
25 chemical composition is still under more investigation (e.g. Drewnick et al., 2007, Hao et  
26 al., 2013, Wu et al., 2013).

27  
28 Using the ratio of the inorganic mass concentration to the total mass concentration  
29 (inorganic fraction, IO) as a measure of particle composition, Dusek et al. (2006) showed  
30 that ~80% of the particle activation is explained by the particle size distribution and only  
31 20% by particle chemical composition. Kivekäs et al. (2009) found a positive correlation

1 between activation efficiency and IO but IO was also correlated with accumulation mode  
2 particle concentration, making the separation of the effect of chemistry and particle size  
3 complicated.

4  
5 Aerosol hygroscopicity defines how the particles grow at an elevated relative humidity  
6 and in the presence of a cloud. The distribution of the hygroscopic growth factor ( $GF_H$ ),  
7 determined as the ratio of wet to dry aerosol particle diameter, can be used as an indicator  
8 of the presence of less and more hygroscopic particles and thus, the aerosol mixing state.  
9 However,  $GF_H$  depends also on particle size (e.g. Sjogren et al., 2008, Kammermann et  
10 al., 2010, Fors et al., 2011), which is due to the Kelvin effect: for smaller particles, the  
11 partial pressure of water vapor on the more curved particle surface is higher, thus  
12 inhibiting the condensation of water. Furthermore, smaller particles are often less  
13 hygroscopic than larger particles, which are aged and possibly cloud processed.

14  
15 So far, long-term in-situ observations on aerosol-cloud interactions are available only  
16 from a few measurement stations, e.g. the Global Atmospheric Watch stations at Pallas,  
17 Finland (e.g. Komppula et al., 2005) and Jungfraujoch, Switzerland (e.g. Henning et al.,  
18 2002) as well as the SMEAR (Station for Measuring Forest Ecosystem-Atmosphere  
19 Relations) IV station at Puijo, Finland (Leskinen et al., 2009, Portin et al., 2009, Hao et  
20 al., 2013, Ahmad et al., 2013). Puijo is located in a semiurban environment, which makes  
21 it easier to investigate the effects of local pollutant sources and therefore the effect of  
22 aerosols with different chemical composition on aerosol-cloud interactions. In this paper  
23 we present the results from two intensive measurement campaigns (Puijo Aerosol Cloud  
24 Experiment, PuCE, 20 September-22 October 2010 & 26 September-31 October 2011)  
25 and provide new, detailed information about the effect of aerosols with different origins  
26 and chemical composition on the particle activation process in liquid water clouds.

## 27 **2 Methods**

### 29 **2.1 Site description**

1 The Puijo station resides on the top floor of the Puijo observation tower (62°54'32'' N,  
2 27°39'31'' E, 306 m above sea level, 224 m above the surrounding lake level), which is  
3 located in the city of Kuopio (105000 inhabitants), in a semi-urban environment. Kuopio  
4 is situated in Eastern Finland, about 330 km to the Northeast from Helsinki. A map of the  
5 location of Kuopio and the area surrounding the tower is shown in Fig. 1, including the  
6 most important local sources: a paper mill in the north, the city center in the southeast, a  
7 heating plant in the south and a highway in the east in north-south direction. Also,  
8 residential areas of different sizes surround the tower, with the biggest in the east and  
9 south and smaller in the southwest, west and northwest. All local sources are located  
10 within 10 km from the tower at approximately 200 m lower altitude than the  
11 measurement level (Table 1). A more detailed overview of the station and the  
12 surrounding area can be found in Leskinen et al. (2009).

13

## 14 **2.2 Cloud events**

15

16 A cloud event is considered to take place at Puijo when the visibility at the top of the  
17 tower drops below 200 meters. Below this limit the cloud and particle activation  
18 properties have been observed to be stable, providing data with best possible quality.  
19 (Portin et al., 2009). The clouds with a visibility above 200 meters may already be non-  
20 uniform and the time resolution of the twin-inlet system is not enough to distinguish  
21 quickly varying particle properties. Furthermore, cloud events (or cloud event hours, see  
22 Sect. 2.4) are classified as rainy if the average rain intensity exceeds 0.2 mm/h. This  
23 classification is necessary, since rain drops remove both unactivated aerosol particles and  
24 cloud droplets, thus affecting the data.

25

## 26 **2.3 Instrumentation**

### 27 **2.3.1 Weather parameters**

28

29 The basic weather parameters are measured continuously at Puijo. Visibility and  
30 precipitation are observed with a present weather sensor (Vaisala FD12P). Wind speed

1 and direction are measured with an ultrasonic two-dimensional anemometer (Thies  
2 UA2D). For temperature and relative humidity a Vaisala HMT337 temperature and  
3 relative humidity transmitter is used. All weather instruments are located approximately 2  
4 meters above the roof of the tower except for the anemometer which is in a mast at a  
5 height of 5 meters above the roof to decrease the effect of the tower on measured winds.

### 6 **2.3.2 Twin inlet system**

7  
8 At the Puijo station the aerosol sample is collected with two separate inlets located on the  
9 top of the tower approximately 2.5 meters above the roof. The sample is drawn through  
10 the roof of the tower to the measurement devices which are located in a room on the top  
11 floor.

12  
13 The interstitial inlet has a PM<sub>1</sub> impactor (Digitel DPM10 with a PM<sub>1</sub> nozzle plate for 1  
14 m<sup>3</sup>/h flow rate) to prevent the cloud droplets from entering the sample line. When a cloud  
15 is present, this inlet samples only the interstitial aerosol since the cloud droplets are too  
16 large to enter the sampling line. The residence time of the aerosol sample in the sampling  
17 lines is more than 10 seconds. By the time the sample reaches the measurement devices,  
18 most of the water is evaporated from the particles as the sample air is warmed to the  
19 room temperature (e.g. Hinds, 1999).

20  
21 The total air inlet has a cutoff size of approximately 40 µm. The inlet and the upper part  
22 of the sampling line are heated to 40 °C. Thus, when the tower is in a cloud, the total air  
23 inlet will sample both the cloud droplets and the unactivated, interstitial aerosol particles.  
24 Due to the heating the water from the droplets evaporates, leaving only the residual  
25 particles. This way it is possible to observe the aerosol size distribution as it would be  
26 outside of the cloud.

27  
28 During clear weather, both sampling lines measure the same aerosol distribution if the  
29 aerosol is not changing within 12 minutes measurement cycle. Between the main  
30 sampling lines and the measurement equipment is a valve system consisting of four

1 controllable valves (Comparato, model Diamant 2000) which are used to switch the  
2 measurement devices between the sampling lines in six-minute intervals.

### 3 **2.3.3 Particle size distribution and number concentration**

4

5 Particles in the size range of 7 to 800 nm were measured with a twin differential mobility  
6 particle sizer (twin-DMPS) (Winklmayr et al., 1991, Jokinen and Mäkelä, 1997). One  
7 DMPS measured between 7 to 49 nm with sheath and sample flows of 13.4 and 2 lpm,  
8 and the other from 27 to 800 nm with sheath and sample flows of 5.5 and 1 lpm,  
9 respectively. Flow checks were made periodically. For the size range of 20-200 nm,  
10 where majority of the cloud droplet formation takes place, the accuracy of the DMPS is  
11 estimated to be 10 %, as discussed in Wiedensohler et al. (2012). The instrument was  
12 connected to the twin inlet system all the time and a full size distribution for both  
13 sampling lines was provided with a 12-minute time resolution. The times of the measured  
14 size distributions from interstitial and total lines differ by six minutes, which has to be  
15 considered in the data analysis, normally by averaging over some time period. By  
16 comparing the size distributions between the sampling lines, it is possible to observe the  
17 size dependent cloud droplet activation of the particles.

18  
19 In this study, we defined the nucleation mode particle concentration ( $N_{\text{nuc}}$ ) as the  
20 concentration of particles with a diameter  $D_p < 25$  nm. For Aitken mode particle  
21 concentration ( $N_{\text{ait}}$ ) the corresponding size range is  $25 \text{ nm} < D_p < 100$  nm and for the  
22 accumulation mode concentration ( $N_{\text{acc}}$ )  $D_p > 100$  nm. Moreover,  $D_{50}$  is defined as the  
23 diameter above which at least 50% of the particles have activated into cloud droplets  
24 (Komppula et al., 2005).

### 25 **2.3.4 Cloud droplets**

26

27 Cloud droplets were observed with a cloud droplet probe (CDP, Droplet Measurement  
28 Technologies) with a 10 s time resolution. The CDP measures the cloud droplet size  
29 distribution in the size range of 3 to 50  $\mu\text{m}$  by classifying the droplets into 30 size bins

1 according to the scattered light of a laser beam at a wavelength of 658 nm. The cloud  
2 droplet number concentration in each size bin is calculated by dividing the raw droplet  
3 counts with the volume of air passing through the sampling area of the laser beam. The  
4 instrument has a custom-built tubular inlet with an external pump to provide a constant  
5 sample flow (13 m/s, checked in the beginning of both campaigns). It is mounted on a  
6 swivel, which keeps the inlet facing the wind. The accuracy of the CDP is estimated to be  
7 20%-30%, typical for other devices with the same detection principle (e.g. forward  
8 scattering spectrometer probe, FSSP) (Brenner and Bourriane, 1998). The size  
9 detection of the probe was proven with glass beads of 5 to 40  $\mu\text{m}$  in diameter in the  
10 beginning of both campaigns. The CDP data was also used to estimate the cloud liquid  
11 water content (LWC) by calculating the total volume of the droplet population.

### 12 **2.3.5 Particle chemical composition**

13  
14 The particle chemical composition was studied with an Aerodyne high resolution aerosol  
15 time-of-flight mass spectrometer (HR-ToF-AMS, DeCarlo et al., 2006). An aerodynamic  
16 lens focuses the particles into a narrow beam, which enters a vacuum, where the particles  
17 are flash-vaporized and ionized. The ion fragments are detected by a time-of-flight  
18 mass spectrometer.

19  
20 The aerosol mass spectrometer (AMS) provides the mass concentrations of organics,  
21 sulphate, nitrate, ammonium and chloride in the size range  $40 \text{ nm} < D_p < 1 \mu\text{m}$ . However,  
22 in this study the chloride data is omitted since the concentrations at Puijo were negligible.  
23 The inorganic fraction (IO) is defined as the ratio of the inorganic mass concentration to  
24 the total mass concentration. Twin inlet data for the AMS is available for the whole 2011  
25 campaign. In the 2010 campaign, the AMS was connected to the twin inlet system only  
26 for a period of 28 hours for a case study (Hao et al., 2013), otherwise to the total line. To  
27 get uniform data from both campaigns, AMS data collected from the total line is used  
28 when discussing the whole 2010-2011 data set and twin-inlet data in the case study from  
29 the 2011 campaign.



### 2.3.6 Particle hygroscopicity

A hygroscopicity tandem differential mobility analyzer (H-TDMA, Joutsensaari et al., 2001) was used to observe the hygroscopic growth of aerosol particles during PuCE 2011. In order to measure dry aerosol, the device was connected directly to the total line, instead of switching between the two sampling lines. The setup has a humidifier between the two DMAs. The first DMA selects particles with a certain dry size from the original polydisperse aerosol. In this study, the selected dry sizes were 80, 100 and 150 nm. The monodisperse aerosol enters the humidifier, which is set at 90 % relative humidity. The size distribution of the humid aerosol is measured with the second DMA. From this size distribution the average hygroscopic growth factor ( $GF_H$ , the ratio of wet to dry particle diameter) for a certain dry diameter is calculated. The instrument measures one dry size for five minutes, so a full cycle takes about 15 minutes. As the H-TDMA was operated only for a few days during the 2011 campaign, the data will be presented only for the case study.

Typical values of  $GF_H$  for 100 nm ambient aerosol particles ( $GF_{100}$ ) vary from 1.0 to 1.5 (Sjogren et al., 2008). Black carbon is hydrophobic ( $GF_H = 1.0$ ), organics are less hygroscopic ( $GF_H \approx 1.2$ ) and anthropogenic particles with higher IO are more hygroscopic ( $GF_H > 1.3$ ). The ratio between the number concentrations of more and less hygroscopic particles is defined as  $R_{GF} = N_{GF>1.25}/N_{GF\leq 1.25}$ , where  $N_{GF>1.25}$  and  $N_{GF\leq 1.25}$  are the number concentrations of particles with  $GF_H$  more than and less than or equal to 1.25, respectively. The limit 1.25 was chosen as it represented in most cases the midpoint between the low  $GF_H$  and high  $GF_H$  modes of the hygroscopicity distributions of this study and the same limit was also used in Kammermann et al. (2010).

### 2.4 Data evaluation

As the first step of the data analysis, one-hour averages were calculated for the whole data set from both 2010 and 2011 campaigns, except for the CDP, for which the 10-

1 second data were used. The averaging was done in order to even out discrepancies in the  
2 twin-DMPS size distributions between the sampling lines.

3  
4 The hours with average visibility below 200 meters were classified as cloud event hours.  
5 For the case study (Sect. 3.3), instead of hourly averages, the data were averaged over the  
6 different subperiods.

7  
8 An hour was classified as a clear hour if the average relative humidity was below 80 %  
9 or the average height of the lowest cloud layer, measured by a ceilometer (Vaisala  
10 CT25K) located in a nearby weather station, was over 500 m (~300 m above the top of  
11 the tower). The choice to use these criteria instead of some high value for visibility was  
12 made because even at visibilities > 40 km, relative humidities higher than 90 % were  
13 sometimes observed, which is enough to have a noticeable effect on the twin inlet data.

14  
15 To study the possible effects of the different local sources, the area surrounding the tower  
16 was divided into five sectors according to the local sources described in Chap. 2.1 (Table  
17 1). The same sectors are also used in Leskinen et al. (2012). It must be noted that the  
18 local sources reside some 200 meters lower, excluding the heating plant and paper mill,  
19 whose emission heights are about 80 and 128 meters lower than the measurement  
20 altitude.

## 21 **3 Results & discussion**

### 22 23 **3.1 Overview of cloud events**

24  
25 During PuCE 2010 and 2011, 39 cloud events were observed, ranging from short periods  
26 of 15 minutes to events lasting up to 31 hours. In total, these events provided 156 cloud  
27 event hours (visibility < 200 m). The majority of the cloud event hours took place when  
28 the wind direction was from sector 3 (69 hours) or sector 5 (50 hours). It is very likely  
29 that the air masses coming from sector 5 are cleaner and of marine origin (Portin et al.,  
30 2009). However, these air masses have spent some time over the continent, which has

1 removed most of the marine characteristics, as indicated by e.g. the absence of chloride.  
2 The air masses from sector 3, on the contrary, are affected by the local sources. Thus,  
3 from now on, the results and discussion presented here will focus on the comparison of  
4 these two sectors, which will be referred as polluted (3) and clean (5) sectors,  
5 respectively.

6

## 7 **3.2 Aerosol-cloud interactions for air masses with and without local** 8 **pollutant sources**

### 9 **3.2.1 Particle size distribution**

10

11 A summary of the aerosol properties for the sectors with and without local pollutant  
12 sources is shown in Table 2 along with the average values calculated from the whole data  
13 set. All the particle data discussed are from the total air inlet, if not mentioned otherwise.  
14 Also the standard error of the mean was calculated for the observations for the times  
15 corresponding to the one-hour averages. The values were calculated for clear ( $RH < 80\%$   
16 or height of the lowest cloud  $> 500$  m) (943 hours in total) and cloudy conditions (156  
17 hours) during the campaigns. The corresponding average size distributions are shown in  
18 Fig. 2. The average particle number concentration ( $N_{tot}$ ) in the air mass coming from the  
19 polluted sector in clear conditions ( $2930 \text{ cm}^{-3}$ ) was higher than that of the clean sector  
20 ( $2000 \text{ cm}^{-3}$ ) for all particle sizes. The mean total particle volume concentrations ( $V_{tot}$ )  
21 were  $3.0 \mu\text{m}^3 \text{cm}^{-3}$  and  $0.80 \mu\text{m}^3 \text{cm}^{-3}$  for the polluted and clean sectors, respectively.  
22 Furthermore, the size distribution for the polluted sector was much broader, suggesting  
23 that the particles had originated from multiple sources.

24

25 In cloudy conditions, the mean  $N_{tot}$  decreased by 43 % for the polluted and by 51 % for  
26 the clean sector due to particles impacting into cloud droplets and wet removal.  
27 Scavenging was most significant for nucleation mode particles, leading to an increase in  
28 the geometric mean particle diameters (GMD) of the total aerosol (Fig. 2, Table 2). For  
29 the clean sector the GMD increased by 120 %, which is considerably more than the 16 %  
30 increase for the polluted sector. The  $V_{tot}$  was equal ( $2.5 \mu\text{m}^3 \text{cm}^{-3}$ ) for both sectors in

1 cloudy conditions. For the clean sector the  $V_{\text{tot}}$  in cloudy conditions was three times that  
2 in clear conditions. The differences in the particle populations of the two sectors can be  
3 explained by cloud processing: some of the smaller particles diffuse to droplets and trace  
4 gases convert to particulate matter within the droplets. This increases the size of activated  
5 particles and produces bimodal size distributions when the cloud droplets evaporate.

6  
7 The cloud processing is often most evident in clean, marine aerosol (e.g. Hoppel et al.,  
8 1986, Frick and Hoppel, 1993, Mochida et al., 2011). At Puijo, cloud processing has been  
9 observed in the air masses from both sectors but it was more distinguishable in the air  
10 masses arriving from the clean sector. For the polluted sector the effect of cloud  
11 processing was partly masked by the higher  $N_{\text{tot}}$ . A clear hump can be seen in the clean  
12 sector size distribution at around 200 nm (Fig. 2b), indicating cloud processing. The  
13 hump is also seen in the size distribution measured in clear conditions (Fig. 2a), meaning  
14 that the air masses have gone through cloud formation and processing on their way to  
15 Puijo. For the polluted sector, the hump can also be observed in both clear and cloudy  
16 conditions but it overlaps more with the Aitken mode.

### 17 **3.2.2 Particle activation and cloud droplet size distribution**

18  
19 The average activated fractions as a function of particle diameter for the two sectors were  
20 calculated from the particle size distribution data provided by the twin-DMPS (Fig. 3).  
21 For the polluted sector, even smaller particles activate and the activation curve is less  
22 steep than for the clean sector. The steepness of the activation curve gives information  
23 about the aerosol mixing state (Asmi et al., 2012). A steeper curve, like the one observed  
24 for the clean sector, is an indication of more internally mixed and more aged particles. A  
25 less steep curve means that aerosol from several sources with variable chemical  
26 composition and hygroscopic properties have been present, as is the case for the polluted  
27 sector. The number concentration of activated particles ( $N_{\text{act}}$ , calculated as the  
28 concentration difference between the total and interstitial sampling lines) differed by 21  
29 % between the two sectors, being  $210 \text{ cm}^{-3}$  and  $165 \text{ cm}^{-3}$  for polluted and clean,  
30 respectively (Table 3). However, the size distributions of the activated particles were very

1 similar for both sectors (Fig. 2b). The only difference was that the size distribution for the  
2 polluted sector was tilted towards smaller particle sizes, which also explains the  
3 difference in  $N_{act}$ .

4  
5 The average cloud droplet concentrations provided by the CDP ( $N_d$ ) were 293 and 266  
6  $\text{cm}^{-3}$  for the polluted and clean sectors, respectively. These numbers are comparable to  
7  $N_{act}$  within the instrumental uncertainties of 10 and 30% of the DMPS and CDP,  
8 respectively. The arithmetic mean droplet diameters ( $D_d$ ) were 8.3 and 8.9  $\mu\text{m}$  for the  
9 polluted and clean sectors, respectively (Table 3). Although these differences were small,  
10 this is just what one would expect based on the particle population properties of the two  
11 sectors. Higher  $N_{tot}$ , especially  $N_{acc}$ , of the polluted sector favors more and smaller  
12 droplets. The liquid water contents (LWC) were equal, 0.14  $\text{g m}^{-3}$ , for both sectors.

13  
14 It has to be emphasized that the differences in the properties of activated particles and  
15 cloud droplets between the two sectors are small. Also, there is a lot of variability in the  
16 data, as indicated by the high standard deviations (Table 3). This means that the  
17 interpretation of these data have to be made with caution and that more detailed studies,  
18 like the case study presented in section 3.3, are needed to support the conclusions  
19 presented here.

### 20 **3.2.3 Particle chemical composition**

21  
22 The mass concentrations of the chemical components for the two sectors are shown in  
23 Table 4. In clear conditions, as one would expect based on the larger number of particles,  
24 the average concentrations of all measured constituents (organics,  $\text{SO}_4$ ,  $\text{NO}_3$ ,  $\text{NH}_4$ ) were  
25 higher in the polluted than in the clean air masses. In cloudy conditions compared to the  
26 clear conditions, the  $\text{NO}_3$  concentration was the same but the organics,  $\text{SO}_4$ , and  $\text{NH}_4$   
27 concentrations were lower by 18%, 9%, and 33%, respectively, for the polluted sector.  
28 For the clean sector, as a considerable increase in  $N_{acc}$  took place (Fig. 2), the  
29 concentration of all constituents were higher by a factor of 2...6 compared to the clear  
30 conditions. For  $\text{NO}_3$  the concentration even exceeded that of the polluted sector and for

1 NH<sub>4</sub> the concentrations were equal. The IO was 42...44 % for both sectors and for both  
2 clear and cloudy conditions.

3  
4 The most significant differences in the in-cloud aerosol composition between the two  
5 sectors were the higher concentration of SO<sub>4</sub> for the polluted sector compared to the clean  
6 sector (1.08 vs. 0.69 μg m<sup>-3</sup>) and the lower concentration of NO<sub>3</sub> (0.19 vs. 0.24 μg m<sup>-3</sup>).  
7 The elevated SO<sub>4</sub> may be linked to the local pollutant sources, which produce either SO<sub>4</sub>  
8 particles directly or then SO<sub>2</sub> which is converted into particulate SO<sub>4</sub>. The more acidic  
9 aerosol could also explain the lower NO<sub>3</sub> concentration of the polluted sector.

10  
11 However, based on this analysis, it is impossible to distinguish between the effects of  
12 local sources and possible air mass transport from elsewhere on the polluted sector  
13 aerosol. Furthermore, as was the case with the particle activation and cloud droplet data  
14 discussed in the previous section, also for the particle chemical composition the standard  
15 deviations are large, indicating highly varying aerosol properties.

16

### 17 **3.3 A case study on the effect of local sources on aerosol-cloud** 18 **interactions**

19

20 During PuCE 2011, a long cloud event took place between 22 October, 9:00 and 24  
21 October, 5:15, lasting in total 44 hours. The wind direction, temperature and rain  
22 intensity varied considerably during the event. Also, different air masses and pollutant  
23 plumes from local sources were observed. Thus, it was possible to perform a detailed  
24 analysis on the effects of these variable conditions on aerosol-cloud interactions. The  
25 event could be divided into eight “sub-events” (Table 5). The time series of the most  
26 important weather and other parameters are shown in Figs. 4 and 5.

#### 27 **3.3.1 Rainy period**

28

29 The rainy period, with a southerly wind from the polluted sector, a temperature of slightly  
30 over 0 C° and some rain (on average 0.8 mm/h), was characterized by the highest  $N_{tot}$  of

1 all cloud periods (Table 6). This is mainly explained by a high  $N_{\text{ait}}$  (Fig. 6a), probably  
2 from fresh, anthropogenic emissions.  $N_{\text{acc}}$  was relatively high compared to the other  
3 periods, leading to a high droplet number concentration  $N_{\text{d}}$  with the smallest  $D_{\text{d}}$  of all the  
4 periods. Normally, the droplet size distribution was bimodal, with the first mode around  
5 10  $\mu\text{m}$  and second mode at  $\sim 16 \mu\text{m}$  (Fig. 6d). For this period, however, only the first  
6 mode was observed with a high amount of small droplets. LWC during this period was  
7 the lowest during the whole event, so it is possible that the droplet growth was limited by  
8 the availability of water.

9  
10 The activated fraction of particles for this period remained low, even for the larger  
11 particles, reaching only 80 % (Fig. 6c). This may also have been caused by the removal  
12 of droplets by rain, which affects the particle measurements. Unfortunately, as can be  
13 seen from Figs. 6a and 6c, the low amount of particles in the upper limit of DMPS  
14 measurement range provides poor statistics, wrongly suggesting very low activated  
15 fractions for particles larger than 600 nm in diameter. Furthermore, the particle activation  
16 data in Figs. 6b and 6c suggests that also the smallest particles contributed to droplet  
17 formation. This inaccuracy was likely caused by the large variation in the concentrations  
18 of small particles, the 6-minute time difference between the interstitial and total sampling  
19 lines and for some of the periods, the short averaging time. This has to be kept in mind  
20 when interpreting Fig. 6b and 6c and hence the data for particles smaller than 80 nm in  
21 diameter is illustrated with dashed lines.

22  
23 The chemical composition of particles was dominated by organics, with the  
24 concentrations of other components remaining low (Table 7). The activated fraction of  
25 organics was the lowest for all periods. Also, the particles during this period had a low  
26 average hygroscopicity (Table 8) with very low  $R_{\text{GF}}$  indicating a strong contribution from  
27 the low  $\text{GF}_{\text{H}}$  particles. The growth factor distribution was clearly bimodal, especially for  
28 the 80 nm particles (Figs. 6e, f). It is likely that the nonhygroscopic mode consisted of  
29 particles containing organics or black carbon, some of which remained unactivated. The  
30 largest residential areas and a majority of the traffic in Kuopio are concentrated to the  
31 south from the tower. Both biomass burning and traffic related combustion aerosols are

1 known to be less hygroscopic (Herich et al., 2009). This could also partly explain the low  
2 activated fraction.

### 3 **3.3.2 Clean period**

4

5 During the clean period, air masses were coming from the clean sector, there was no rain  
6 and the temperature dropped below 0 °C. The air was very clean, containing aged aerosol  
7 with low  $N_{\text{tot}}$  and  $N_{\text{acc}}$ . (Table 6). Also, there were no nucleation mode particles, which  
8 was already shown to be typical for this wind sector (Fig. 2). A low  $N_{\text{acc}}$  led to the lowest  
9  $N_{\text{d}}$  of all the periods and a large  $D_{\text{d}}$ .

10

11 The mass concentrations of inorganic components were somewhat higher during this  
12 period compared to the rainy period (Table 7). Also, their activated fraction was higher,  
13 meaning that a larger fraction of them was found in the accumulation mode particles.  
14 This suggests that the air mass was aged and had gone through some cloud processing,  
15 producing internally mixed aerosol before arriving to Puijo. This is also supported by  
16 high values for the hygroscopic growth factors (Table 8). The hygroscopicity distribution  
17 was dominated by the more hygroscopic mode, especially for the 100 and 150 nm  
18 particles as indicated by the high  $R_{\text{GF}}$  values. The  $R_{\text{GF}}$  of 100 and 150 nm particles was  
19 also strongly dependent on the concentration of  $\text{SO}_4$ . In the beginning of the period,  $\text{SO}_4$   
20 was almost absent but throughout the period, its mass fraction increased to 45 %.  $R_{\text{GF}}$  was  
21 around 2 and 6 in the beginning of the period but towards the end increased to 7 and 40  
22 for 100 and 150 nm particles, respectively (Figs. 5c, 7). The average  $\text{GF}_{100}$  was 1.42,  
23 comparable with the Jungfraujoch free tropospheric aerosol, which is also aged and  
24 internally mixed (Sjogren et al., 2008, Kammermann et al., 2010).

### 25 **3.3.3 Paper mill period**

26

27 This short 30-minute period was characterized by a heavy pollution plume from the  
28 nearby paper mill. There was no rain and the temperature was below 0 C°. The particle  
29 population properties differed greatly from those observed during the other periods.  $N_{\text{tot}}$



1 was very low but  $N_{\text{acc}}$  was elevated (Table 6). Due to the pronounced accumulation mode,  
2 a very high  $D_{50}$ , 202 nm, was observed, compared to the normal  $D_{50}$  at Puijo of around  
3 120 nm, as was the case during the first two periods.

4  
5 A time series of the cloud droplet data for the whole cloud event is shown in Fig. 5b.  
6 During the paper mill plume  $N_d$  increased momentarily, coinciding with a quick decrease  
7 in the average droplet size. This sharp change in the droplet population properties is  
8 mainly explained caused by the high  $N_{\text{acc}}$  but the possibility that the different chemical  
9 composition of particles also played a role cannot be excluded. The inorganic  
10 components all experienced a drastic increase, with  $\text{SO}_4$  dominating the composition  
11 (Table 7). Growth factor distributions also showed elevated hygroscopicity for the high-  
12  $\text{GF}_H$  mode, especially for the larger particles (Fig. 6f). However, the presence of a low-  
13  $\text{GF}_H$  mode, probably containing soot particles, lowered the average hygroscopicities  
14 during the plume (Table 8). For example, the average  $\text{GF}_{100}$  was 1.37, whereas for the  
15 high-hygroscopicity mode it was around 1.6. It has to be noted, though, that only one or  
16 two hygroscopicity measurements for each particle size were available for this very short  
17 period, so the  $\text{GF}_H$  values likely have large uncertainties and have to be treated with  
18 caution.

### 19 **3.3.4 Clean 2 period**

20  
21 In the beginning of this period, the wind direction shifted back to the north, fluctuating  
22 between the clean sector and sector 1, with no rain and a temperature of just below 0 C°.  
23 This period shared many similarities with the clean period.  $N_{\text{tot}}$  was even lower,  
24 nucleation mode particles were absent and a pronounced accumulation mode was  
25 observed (Fig. 6a, Table 6), indicating that strong cloud processing had taken place  
26 before the air mass arrived to Puijo.

27  
28 The main difference compared with the clean period was an elevated inorganic mass  
29 concentration, largely due to 2...3 times higher  $\text{SO}_4$  and  $\text{NH}_4$  concentrations (Table 7).  
30 This indicates that the air mass has probably encountered some anthropogenic influence

1 on its way to Puijo, but not from nearby sources. This had a clear influence on particle  
2 hygroscopicity, as seen from the high  $GF_H$  and  $R_{GF}$  values (Table 8) but not on cloud  
3 droplet activation.  $N_d$  was 10 % higher than during the clean period (Table 6) which is of  
4 similar magnitude as the difference in  $N_{acc}$  between the periods.

### 5 **3.3.5 Heating plant period**

6  
7 The period started with a rapid shift in the wind direction from north to south and the  
8 polluted sector. The temperature was still slightly below 0 C°. At the same time, a heavy  
9 pollutant plume from the heating plant reached the tower. The particle population  
10 consisted of pronounced nucleation and accumulation modes (Fig. 6a).  $N_{acc}$  was the  
11 highest of all the periods, and the particles consisted mainly of  $SO_4$  (Fig. 5c). Also, as the  
12 aerosol was highly acidic, the  $NO_3$  concentration was very low. The plume also contained  
13 an exceptionally high amount of  $SO_2$  (Fig. 5d), so it is likely that the majority of the  $SO_4$   
14 observed in the activated particles was formed from  $SO_2$  as a result of cloud processing.  
15 However,  $SO_4$  also dominated the composition of cloud interstitial particles. Since the  
16 smaller, inactivated particles are also liquid at high RH, it is possible that cloud  
17 processing from  $SO_2$  to  $SO_4$  took place also in the interstitial aerosol. Another  
18 explanation is that a part of the  $SO_4$  particles was formed already at the heating plant.

19  
20 The conclusions about particle activation parameters for this period have to be made  
21 carefully as the time resolution of the distribution scan is not good enough to capture the  
22 observed rapid changes in the aerosol properties. For example,  $D_{50}$  was very high, 273  
23 nm, (Table 6) but this does not necessarily represent the actual size of the activating  
24 particles. The activated fraction of particles as a function of size (Fig. 6c) showed a  
25 bimodal behavior. Particles with a diameter of around 100 nm already started activating,  
26 similar to some other periods, but reached only an activation fraction of 40 % at 150 nm.  
27 After this there is a dip in the curve as the heating plant particles started to affect the  
28 activation curve and produced a seemingly high  $D_{50}$ .

29

1 The  $GF_H$  distributions showed a clear bimodal behavior, with the high- $GF_H$  mode slightly  
2 elevated by the heating plant particles. The low mode was also pronounced, and for 100  
3 and 150 nm particles, similar to the observations during the rainy period, indicating  
4 emissions from traffic and residential areas. For 80 nm particles there was a clear  
5 increase in the low  $GF_H$  mode, indicating that the plume contained significant amounts of  
6 small particles with low hygroscopicity, likely soot. Since both hygroscopicity modes  
7 were affected by the plume,  $R_{GF}$  remained moderate. Unfortunately the CDP was frozen  
8 shortly after the beginning of the period, making analysis of the cloud properties  
9 impossible.

### 10 **3.3.6 Southern 1 period**

11

12 During this period, the conditions returned back to normal as the heating plant plume  
13 passed the tower. The temperature rose above 0 C° during the period and the wind direction  
14 was still from the south and the polluted sector. Similar nucleation and Aitken modes  
15 were present as during the heating plant plume (Fig. 6a). For the chemical components  
16 the concentrations were quite normal (Table 7). The  $GF_H$  distributions were similar to  
17 those observed during the rainy period with bimodal shapes and moderate average  $GF_H$   
18 and  $R_{GF}$  (Table 8). As the heating plant had no effect on data during the rainy period, it is  
19 likely that this was the case also here. Thus, southern 1 can be considered to represent  
20 normal “semipolluted” conditions for this sector when the effects of the heating plant and  
21 weather are minor. The CDP was still frozen part of the time, so no reliable droplet data  
22 is available.

### 23 **3.3.7 Southern 2 period**

24

25 After a short clear period, the tower was again covered in cloud with southerly wind and  
26 a temperature of above 0 C°. The aerosol during this period was moderately affected by  
27 the heating plant, indicated by the elevated  $SO_4$  and  $SO_2$  concentrations (Fig. 5). Also the  
28 concentration of organics was higher than during the earlier periods, which might already  
29 be related to the transportation of organic aerosol which was more pronounced during the

1 next period, southern 3. The presence of two different kinds of aerosols had some effect  
2 on the activation of particles. The activated fraction curve was less steep than for most of  
3 the other periods and the size distribution of activated particles was broader (Figs. 5b, c).  
4 Also bimodal  $GF_H$  distributions and low  $R_{GF}$  indicated the presence of externally mixed  
5 aerosol.  $R_{GF}$  also (Fig. 7) correlated with  $SO_4$  and  $SO_2$  concentrations, with higher values  
6 in the middle of the period.

7  
8 The cloud droplet size distribution was unimodal, similar to the rainy period. This  
9 suggests that the unimodality is an occasional feature for southerly clouds and not related  
10 to removal of droplets by rain as suggested for the rainy period. However, this does not  
11 exclude the possibility that rain removal of droplets was taking place during the rainy  
12 period.  $N_d$  during this period was higher despite a lower  $N_{acc}$  compared to the rainy period  
13 (Table 6).

### 14 **3.3.8 Southern 3 period**

15  
16 During southern 3 period, wind was still blowing from the south. The period started with  
17 a drop in the mass concentration of  $SO_4$  and in the concentration of  $SO_2$  (Fig. 5). At the  
18 same time, the organic mass concentration increased to the highest value during the  
19 whole event (Table 7). The rise in the amount of organics was explained by an increase in  
20  $N_{acc}$ , although  $N_{tot}$  remained lower than during other southern periods. As the chemical  
21 composition and  $N_{tot}$  showed little variance during the period (Fig. 5), this would suggest  
22 that the effect of local sources was minor. It is likely that these large organic particles  
23 were transported to Puijo from somewhere else.

24  
25 These organic particles were also characterized by low hygroscopicity (Table 8). For 80  
26 nm particles the hygroscopicity distribution was unimodal with one broad peak centered  
27 at  $GF_H = 1.1$ . Also for the 150 nm particles the low and high hygroscopicity peaks were  
28 broader than for the other periods. (Figs. 6e, f). It is possible that some of the larger  
29 particles remained unactivated because of this, as suggested by the unusually high  $D_{50}$

1 (Table 6). The availability of water was not a limiting factor. Although  $N_d$  was quite  
2 normal, the droplets were the largest and LWC the highest of all the periods.

### 3 4 **3.4 Ratio of inorganics to total mass**

5  
6 Also shown in Table 7 is the IO from the AMS measurements for each of the periods. IO  
7 was the lowest for the rainy and southern 3 periods, 34 and 38 %, respectively, and  
8 higher for the clean, clean 2, southern 1 and southern 2 periods, 59, 64, 51 and 54 %,  
9 respectively. The highest IOs were observed during the paper mill and heating plant  
10 plumes, 85 and 87 %, respectively. The differences between the periods were  
11 considerably larger than those between the different air masses analyzed in Dusek et al.  
12 (2006) (18...42 %) and Kivekäs et al. (2009) (23...44 %). This further supports our  
13 findings that the local pollutant sources have a potential to affect aerosol-cloud  
14 interactions also through the particle chemical composition.

## 15 16 **4 Summary and conclusions**

17  
18 Aerosol-cloud interactions were investigated during two intensive measurement  
19 campaigns at Puijo measurement site during autumns 2010-2011. The object was to find  
20 out the possible effects of local pollutant sources and particle chemical composition on  
21 aerosol-cloud interactions. The first approach was to compare data from two different  
22 wind direction sectors for the whole data set. One sector was considered to be clean, with  
23 no nearby aerosol sources. The other sector was affected by local pollutant sources,  
24 including residential areas, traffic and a heating plant.

25  
26 In clear conditions, the total particle number concentration and the accumulation mode  
27 concentration were 2930 and 580  $\text{cm}^{-3}$  for the polluted and 2000 and 146  $\text{cm}^{-3}$  for the  
28 clean sector, respectively. In cloudy conditions cloud processing took place, leading to  
29 lower total particle concentrations, 1680 and 972  $\text{cm}^{-3}$ , for the polluted and clean air,  
30 respectively. However, unlike for the polluted sector (438  $\text{cm}^{-3}$ ), the accumulation mode

1 concentration increased for the clean sector ( $349 \text{ cm}^{-3}$ ), indicating stronger cloud  
2 processing. The in-cloud mass concentrations of particle chemical components in  
3 polluted air were 1.79, 1.08, 0.19 and  $0.27 \mu\text{g m}^{-3}$  for organics,  $\text{SO}_4$ ,  $\text{NO}_3$  and  $\text{NH}_4$ ,  
4 respectively, and the corresponding numbers for the clean air were 1.61, 0.69, 0.24 and  
5  $0.27 \mu\text{g m}^{-3}$ . . The main difference was the higher amount of sulfates for the polluted  
6 sector. Despite of some differences in the particle properties, the droplet activation  
7 behavior was surprisingly similar for the two sectors. The average diameter where 50 %  
8 of the particles activated were 170 and 164 nm for the polluted and clean air,  
9 respectively. For the polluted sector the average droplet concentration was higher (293  
10 vs.  $266 \text{ cm}^{-3}$ ) and the average diameter smaller (8.3 vs.  $8.9 \mu\text{m}$ ) than for the clean sector.

11

12 The second approach was a case study of a cloud event with variable conditions. The  
13 wind was blowing from both the clean and polluted sectors and plumes from the local  
14 heating plant and paper mill were observed. The total ( $754\text{...}2200 \text{ cm}^{-3}$ ) and accumulation  
15 mode ( $114\text{...}169 \text{ cm}^{-3}$ ) particle concentrations were clearly elevated for the polluted  
16 sector compared to the clean sector ( $214\text{...}451 \text{ cm}^{-3}$  and  $62\text{...}83 \text{ cm}^{-3}$ , respectively). This  
17 also created large differences in the droplet properties, with higher concentrations  
18 ( $197\text{...}234 \text{ cm}^{-3}$  vs.  $138\text{...}152 \text{ cm}^{-3}$ ) and generally smaller droplet mean diameters  
19 ( $9.2\text{...}12.4$  vs.  $11.8\text{...}12.2 \mu\text{m}$ ) for the polluted sector compared to the clean sector,  
20 respectively.

21

22 Aged, cloud processed air masses from the clean sector typically resulted in an internally  
23 mixed, more hygroscopic aerosol with an inorganic fraction of ca. 60 % and hygroscopic  
24 growth factor at 90% for 100 nm particles ( $\text{GF}_H$ ) of 1.42...1.45 With southerly winds, the  
25 particle hygroscopicity distributions were clearly bimodal with one mode centered around  
26  $\text{GF}_H = 1.0$  and the other mode between  $\text{GF}_H = 1.4\text{...}1.5$ , suggesting externally mixed  
27 aerosols. Likely sources for the less hygroscopic particles include local domestic wood  
28 combustion and traffic. The concentration of organics was higher, as indicated by the  
29 lower inorganic fraction, 30...50 %.

30

1 The paper mill plume was short in duration but a high accumulation mode particle  
2 concentration ( $139 \text{ cm}^{-3}$ ) was observed, leading to a momentary increase in droplet  
3 concentration ( $240 \text{ cm}^{-3}$ ) and a decrease in droplet size ( $10.9 \text{ }\mu\text{m}$ ). The heating plant  
4 plume caused an even bigger increase in the accumulation mode concentration ( $169 \text{ cm}^{-3}$ ).  
5 In both the paper mill and the heating plant plumes, elevated amounts of  $\text{SO}_4$  ( $2.46$   
6 and  $4.43 \text{ }\mu\text{g m}^{-3}$ ) and  $\text{NH}_4$  ( $0.99$  and  $0.52 \text{ }\mu\text{g m}^{-3}$ ) were observed, respectively, leading to  
7 inorganic fractions of over 80 %. Unlike the paper mill plume, the heating plant plume  
8 also contained a large amount of  $\text{SO}_2$ . Thus, the  $\text{SO}_4$  from the heating plant was formed  
9 from  $\text{SO}_2$  as a result of cloud processing. For the paper mill plume, the  $\text{SO}_4$  particles were  
10 either generated at the mill or then  $\text{SO}_2$  was present to a lesser extent and was completely  
11 transformed into particulate  $\text{SO}_4$  before arriving to Puijo. Another difference was the  $\text{NO}_3$   
12 concentration, which was elevated in the paper mill plume ( $0.42 \text{ }\mu\text{g m}^{-3}$ ) but very low in  
13 the heating plant plume ( $0.08 \text{ }\mu\text{g m}^{-3}$ ) due to highly acidic aerosol. In both plumes,  
14 elevated amounts of more hygroscopic particles ( $\text{GF}_H = 1.5\text{--}1.6$ ) were observed in  
15 addition to smaller, hydrophobic soot particles ( $\text{GF}_H = 1.0$ ).

16

17 As a conclusion, the case study presented here supported and complemented the results  
18 from the sector comparison and the main results from these two methods can be  
19 summarized as follows: 1) The particle concentration in aged, cloud-processed, internally  
20 mixed and more hygroscopic air masses is low but a pronounced accumulation mode is  
21 present, leading to fewer cloud droplets with larger size. 2) Air masses affected by local  
22 sources contain more nucleation and Aitken mode particles with lower hygroscopicity.  
23 The aerosol is externally mixed with a higher inorganic content. The cloud droplets are  
24 smaller but more numerous. 3) Local point sources have the potential to affect aerosol-  
25 cloud interactions both through an increased particle concentration and through their  
26 effect on chemistry.

27

## 28 **Acknowledgements**

29

30 This work was partly supported by the Academy of Finland (Centre of Excellence, No  
31 1118615 and decision number 267514), and the strategic funding of the University of

1 Eastern Finland. Hao, L. acknowledges the financial support of UEF Postdoc Research  
2 Foundation (No. 930275).

3  
4  
5  
6  
7  
8  
9  
10  
11  
12  
13  
14  
15  
16  
17  
18  
19  
20  
21  
22  
23  
24  
25  
26  
27  
28  
29  
30  
31



## 1 **References**

2  
3 Ahmad, I., Mielonen, T., Grosvenor, D. P., Portin, H., Arola, A., Mikkonen, S., Kühn, T.,  
4 Leskinen, A., Joutsensaari J., Komppula, M., Lehtinen, K. E. J., Laaksonen, A., and  
5 Romakkaniemi, S.: Long-term measurements of cloud droplet concentrations and  
6 aerosol-cloud interactions in continental boundary layer clouds, *Tellus B*, 65, 20138,  
7 <http://dx.doi.org/10.3402/tellusb.v65i0.20138>, 2013

8  
9 Albrecht, B. A.: Aerosols, cloud microphysics, and fractional cloudiness, *Science*, 245,  
10 1227-1230, 1989.

11  
12 Anttila, T., Vaattovaara, P., Komppula, M., Hyvärinen, A.-P., Lihavainen, H., Kerminen,  
13 V.-M., and Laaksonen, A.: Size-dependent activation of aerosols into cloud droplets at a  
14 subarctic background site during the second Pallas Cloud Experiment (2nd PaCE):  
15 method development and data evaluation, *Atmos. Chem. Phys.*, 9, 4841-4854, 2009.

16  
17 Asmi, E., Freney, E., Hervo, M., Picard, D., Rose, C., Colomb, A., and Sellegri, K.:  
18 Aerosol cloud activation in summer and winter at puy-de-Dôme high altitude site in  
19 France, *Atmos. Chem. Phys.*, 12, 11589-11607, 2012.

20  
21 Brenguier, J.-L., and Bourriane, T.: Improvements of Droplet Size Distribution  
22 Measurements with the Fast-FSSP (Forward Scattering Spectrometer Probe), *J. Atmos.*  
23 *Ocean. Tech.*, 15, 1077-1090, 1998.

24  
25 Brenguier, J.-L., Pawlowska, H., and Schuller, L.: Cloud microphysical and radiative  
26 properties for parameterization and satellite monitoring of the indirect effect of aerosols  
27 on climate, *J. Geophys. Res.*, 108(D15), 8632, doi:10.1029/2002JD002682, 2003.

28  
29 Coakley, J. A., and Walsh, C. D.: Limits to the aerosol indirect effect derived from  
30 observations of ship tracks, *J. Atmos. Sci.*, 59, 668-680, 2002.

31

1 DeCarlo, P. F., Kimmel, J. R., Trimborn, A., Northway, M. J., Jayne, J. T., Aiken, A. C.,  
2 Gonin, M., Fuhrer, K., Horvath, T., Docherty, K. S., Worsnop, D. R., and Jimenez, J. L.:  
3 Field-deployable, high-resolution, time-of-flight aerosol mass spectrometer, *Anal. Chem.*,  
4 78 (24), 8281-8289, 2006.

5

6 Drewnick, F., Schneider, J., Hings, S. S., Hock, N., Noone, K., Targino, A., Weimer, S.,  
7 and Borrmann, S.: Measurement of ambient, interstitial, and residual aerosol particles on  
8 a mountaintop site in central Sweden using an aerosol mass spectrometer and a CVI, *J.*  
9 *Atmos. Chem.*, 56, 1-20, 2007.

10

11 Dusek, U., Frank, G. P., Hildebrandt, L., Curtius, J., Schneider, J., Walter, S., Chand, D.,  
12 Drewnick, F., Hings, S., Jung, D., Borrmann, S., and Andreae, M. O.: Size matters more  
13 than chemistry for cloud-nucleating ability of aerosol particles, *Science*, 312, 1375-1378,  
14 2006.

15

16 Fors, E. O., Swietlicki, E., Svenningsson, B., Kristensson, A., Frank, G. P., and Sporre,  
17 M.: Hygroscopic properties of the ambient aerosol in southern Sweden - a two year study,  
18 *Atmos. Chem. Phys.*, 11, 8343-8361, 2011.

19

20 Frick, G. M., and Hoppel, W. A.: Airship Measurements of Aerosol Size Distributions,  
21 Cloud Droplet Spectra, and Trace Gas Concentrations in the Marine Boundary Layer, *B.*  
22 *Am. Meteorol. Soc.*, 74, 2195-2202, 1993.

23

24 Han, Q., Rossow, W. B., Zeng, J., and Welch, R.: Three different behaviors of liquid  
25 water path of water clouds in aerosol-cloud interactions, *J. Atmos. Sci.*, 59, 726-735,  
26 2002.

27

28 Hao, L. Q., Romakkaniemi, S., Kortelainen, A., Jaatinen, A., Portin, H., Miettinen, P.,  
29 Komppula, M., Leskinen, A., Virtanen, A., Smith, J. N., Sueper, D., Worsnop, D. R.,  
30 Lehtinen, K. E. J., and Laaksonen, A.: Aerosol Chemical Composition in Cloud Events

1 by High Resolution Time-of-Flight Aerosol Mass Spectrometry, *Environ. Sci. Technol.*,  
2 47, 2645-2653, 2013.

3

4 Henning, S., Weingartner, E., Schmidt, S., Wendisch, M., Gäggeler, H. W., and  
5 Baltensperger, U.: Size-dependent aerosol activation at the high-alpine site Jungfraujoch  
6 (3580 m a.s.l), *Tellus B*, 54, 82-95, 2002.

7

8 Herich, H., Kammermann, L., Friedman, B., Gross, D. S., Weingartner, E., Lohmann, U.,  
9 Spichtinger, P., Gysel, M., Baltensperger, U., and Cziczo, D. J.: Subarctic atmospheric  
10 aerosol composition: 2. Hygroscopic growth properties, *J. Geophys. Res.*, 114, D13204,  
11 doi:10.1029/2008JD011574, 2009.

12

13 Hinds, W. C.: *Aerosol Technology. Properties, Behavior and Measurement of Airborne*  
14 *Particles*. New York, USA: Wiley Interscience.

15

16 Hoppel, W. A., Frick, G. M., and Larson, R. E.: Effect of nonprecipitating clouds on the  
17 aerosol size distribution in the marine boundary layer, *Geophys. Res. Lett.*, 13, 125-128,  
18 1986.

19

20 Hudson, J. G.: Variability of the relationship between particle size and cloud-nucleating  
21 ability, *Geophys. Res. Lett.*, 34, L08801, doi:10.1029/2006GL028850, 2007.

22

23 IPCC 2013. *Climate change 2013: The physical science basis*. Intergovernmental panel  
24 on Climate Change, Cambridge University Press, New York.

25

26 Jokinen, V., and Mäkelä, J. M.: Closed-loop arrangement with critical orifice for DMA  
27 sheath/excess flow system, *J. Aerosol Sci.*, 28, 643-648, 1997.

28

29 Joutsensaari, J., Vaattovaara, P., Vestervinen, M., Hämeri, K., and Laaksonen, A.: A novel  
30 tandem differential mobility analyzer with organic vapor treatment of aerosol particles,  
31 *Atmos. Chem. and Phys.*, 1, 51-60, 2001.

1 Kammermann, L., Gysel, M., Weingartner, E., and Baltensperger, U.: 13-month  
2 climatology of the aerosol hygroscopicity at the free tropospheric site Jungfraujoch (3580  
3 m a.s.l.), *Atmos. Chem. Phys.*, 10, 10717-10732, 2010.  
4  
5 Kivekäs, N., Kerminen, V.-M., Raatikainen, T., Vaattovaara, P., Laaksonen, A., and  
6 Lihavainen, H.: Physical and chemical characteristics of aerosol particles and cloud-  
7 droplet activation during the Second Pallas Cloud Experiment (Second PaCE), *Boreal*  
8 *Environ. Res.*, 14, 515-526, 2009.  
9  
10 Komppula, M., Lihavainen, H., Kerminen, V.-M., Kulmala, M., and Viisanen, Y.:  
11 Measurements of cloud droplet activation of aerosol particles at a clean subarctic  
12 background site, *J. Geophys. Res.*, 110, D06204, doi:10.1029/2004JD005200, 2005.  
13  
14 Leskinen, A., Portin, H., Komppula, M., Miettinen, P., Arola, A., Lihavainen, H.,  
15 Hatakka, J., Laaksonen, A., and Lehtinen, K. E. J.: Overview of the research activities  
16 and results at Puijo semi-urban measurement station, *Boreal Environ. Res.*, 14, 576-590,  
17 2009.  
18  
19 Leskinen, A., Arola, A., Komppula, M., Portin, H., Tiitta, P., Miettinen, P.,  
20 Romakkaniemi, S., Laaksonen, A., and Lehtinen, K. E. J.: Seasonal cycle and source  
21 analyses of aerosol optical properties in a semi-urban environment at Puijo station in  
22 Eastern Finland, *Atmos. Chem. Phys.*, 12, 5647–5659, 2012.  
23  
24 Lohmann, U., and Feichter, J.: Global indirect aerosol effects: a review, *Atmos. Chem.*  
25 *Phys.*, 5, 715-737, 2005.  
26  
27 Menon, S., Del Genio, A. D., Koch, D., and Tseloudis, G.: GCM simulations of the  
28 aerosol indirect effect: sensitivity to cloud parameterization and aerosol burden, *J. Atmos.*  
29 *Sci.*, 59, 692-713, 2002.  
30

1 Mochida, M., Nishita-Hara, C., Furutani, H., Miyazaki, Y., Jung, J., Kawamura, K., and  
2 Uematsu, M.: Hygroscopicity and cloud condensation nucleus activity of marine aerosol  
3 particles over the western North Pacific, *J. Geophys. Res.*, 116, D06204,  
4 doi:10.1029/2010JD014759, 2011.  
5  
6 Portin, H., Komppula, M., Leskinen, A., Romakkaniemi, S., Laaksonen, A., and  
7 Lehtinen, K. E. J.: Observations of aerosol-cloud interactions at Puijo semi-urban  
8 measurement station, *Boreal Environ. Res.*, 14, 641-653, 2009.  
9  
10 Rotstajn, L. D., and Liu, Y.: A smaller global estimate of the second indirect aerosol  
11 effect, *Geophys. Res. Lett.*, 32, L05708, doi:10.1029/2004GL021922, 2005.  
12  
13 Sekiguchi, M., Nakajima, T., Suzuki, K., Kawamoto, K., Higurashi, A., Rosenfeld, D.,  
14 Sano, I., and Mukai, S.: A study of the direct and indirect effects of aerosols and cloud  
15 parameters, *J. Geophys. Res.*, 108(D22), 4699, doi:10.1029/2002JD003359, 2003.  
16  
17 Sjogren, S., Gysel, M., Weingartner, E., Alfarra, M. R., Duplissy, J., Cozic, J., Crosier, J.,  
18 Coe, H., and Baltensperger, U.: Hygroscopicity of the submicrometer aerosol at the high-  
19 alpine site Jungfrauoch, 3580 m a.s.l., Switzerland, *Atmos. Chem. Phys.*, 8, 5715-5729,  
20 2008.  
21  
22 Twomey, S.: The influence of pollution on the shortwave albedo of clouds, *J. Atmos.*  
23 *Sci.*, 34, 1149-1152, 1977.  
24  
25 Vong, R. J., and Covert, D. S.: Simultaneous observations of aerosol and cloud droplet  
26 size spectra in marine stratocumulus, *J. Atmos. Sci.*, 55, 2180-2190, 1998.  
27  
28 Wang, J., Lee, Y.-N., Daum, P. H., Jayne, J., and Alexander, M. L.: Effects of aerosol  
29 organics on cloud condensation nucleus (CCN) concentration and first indirect aerosol  
30 effect, *Atmos. Chem. Phys.*, 8, 6325-6339, 2008.  
31

1 Winklmayr, W., Reischl, G. P., Linder, A. O., and Berner, A.: A new electromobility  
2 spectrometer for the measurement of aerosol size distribution in the size range 1 to 1000  
3 nm, *J. Aerosol Sci.*, 22, 289-296, 1991.

4

5 Wu, Z. J., Poulain, L., Henning, S., Dieckmann, K., Birmili, W., Merkel, M., van  
6 Pinxteren, D., Spindler, G., Müller, K., Stratmann, F., Herrmann, H., and  
7 Wiedensohler, A.: Relating particle hygroscopicity and CCN activity to chemical  
8 composition during the HCCT-2010 field campaign, *Atmos. Chem. Phys.*, 13, 7983-  
9 7996, 2013.

10

11

12

13

14

15

16

17

18

19

20

21

22

23

24

25

26

27

28

29

30

31

32

33

34

35

36

37

38

39

40

41

42

1 Table 1. Sectors used for data classification and a list of local sources.

2

	Sector	Source	Direction and distance from the tower
1	0...45°	Paper mill	35°, 5 km
		Highway	6...45°, > 1.4 km
2	45...155°	City center	120...155°, 1.6-3.2 km
		Residential areas	45...120°, 1.2-4 km
		Highway	45...155°, 1-1.4 km
3	155...215°	Heating plant	160°, 3.5 km
		Residential areas	155...215°, 3.4-10 km
		Highway	155...192°, > 1 km
4	215...245°	Residential areas	215...245°, 3.4-4 km
5	245...360°	Residential areas	245...360°, 1.5-3.5 km

3

4

5

6

7

8

9

10

11

12

13

14

15

16

17

18

19

20

1 Table 2. Average values and standard deviations of total particle number concentration  
 2 ( $N_{\text{tot}}$ ), geometric mean particle diameter (GMD), total particle volume concentration  
 3 ( $V_{\text{tot}}$ ), number concentrations of nucleation, Aitken and accumulation mode particles  
 4 ( $N_{\text{nuc}}$ ,  $N_{\text{ait}}$ ,  $N_{\text{acc}}$ ) and ratio  $N_{\text{ait}}/N_{\text{acc}}$ . Values are calculated from the twin-DMPS data for  
 5 the sectors with and without local pollutant sources, for the whole data set and for both  
 6 clear and cloudy conditions. Data are from the total sampling line.

7

sector	$N_{\text{tot}}$ ( $\text{cm}^{-3}$ )		GMD (nm)		$V_{\text{tot}}$ ( $\mu\text{m}^3 \text{cm}^{-3}$ )		$N_{\text{nuc}}$ ( $\text{cm}^{-3}$ )		$N_{\text{ait}}$ ( $\text{cm}^{-3}$ )		$N_{\text{acc}}$ ( $\text{cm}^{-3}$ )		$N_{\text{ait}}/N_{\text{acc}}$	
	clear	cloud	clear	cloud	clear	cloud	clear	cloud	clear	cloud	clear	cloud	clear	cloud
polluted	2930	1680	44	51	3.0	2.5	1170	511	1180	727	580	438	3.2	2.8
	$\pm 2030$	$\pm 1020$	$\pm 19$	$\pm 24$	$\pm 2.2$	$\pm 2.7$	$\pm 1780$	$\pm 580$	$\pm 525$	$\pm 436$	$\pm 384$	$\pm 490$	$\pm 3.0$	$\pm 2.3$
clean	2000	972	35	77	0.80	2.5	1040	126	812	498	146	349	9.2	2.5
	$\pm 1510$	$\pm 771$	$\pm 20$	$\pm 30$	$\pm 0.94$	$\pm 2.3$	$\pm 1250$	$\pm 258$	$\pm 578$	$\pm 404$	$\pm 142$	$\pm 291$	$\pm 8.8$	$\pm 2.6$
all	2480	1530	39	59	1.6	2.6	1070	443	1000	669	311	416	6.6	2.6
	$\pm 2440$	$\pm 1100$	$\pm 21$	$\pm 29$	$\pm 1.8$	$\pm 2.4$	$\pm 2120$	$\pm 624$	$\pm 652$	$\pm 452$	$\pm 312$	$\pm 392$	$\pm 7.0$	$\pm 2.6$

8

9

10

11

12

13

14

15

16

17

18

19

20

21

22

23

24

25

26



1 Table 3. Average values and standard deviations of number concentration of activated  
 2 particles ( $N_{\text{act}}$ , calculated as the concentration difference between the total and interstitial  
 3 lines), cloud droplet number concentration ( $N_d$ ), droplet diameter ( $D_d$ ) and liquid water  
 4 content (LWC) in cloudy conditions for the sectors with and without local pollutant  
 5 sources and for the whole data set.

6

sector	$N_{\text{act}}$ ( $\text{cm}^{-3}$ )	$N_d$ ( $\text{cm}^{-3}$ )	$D_d$ ( $\mu\text{m}$ )	LWC ( $\text{g m}^{-3}$ )
polluted	210±148	293±159	8.3±2.3	0.14±0.13
clean	165±126	266±124	8.9±2.2	0.14±0.09
all	209±186	285±168	8.9±2.3	0.15±0.12

7

8

9

10

11

12

13

14

15

16

17

18

19

20

21

22

23

24

25

26

27

1 Table 4. Average mass concentrations and standard deviations of the chemical  
 2 constituents measured by the AMS for the sectors with and without local pollutant  
 3 sources, for the whole data set and for both clear and cloudy conditions. Data are from  
 4 the total sampling line.

5

sector	Organics ( $\mu\text{g m}^{-3}$ )		SO <sub>4</sub> ( $\mu\text{g m}^{-3}$ )		NO <sub>3</sub> ( $\mu\text{g m}^{-3}$ )		NH <sub>4</sub> ( $\mu\text{g m}^{-3}$ )		Inorg/total (%)	
	clear	cloud	clear	cloud	clear	cloud	clear	cloud	clear	cloud
polluted	2.17	1.79	1.19±1.1	1.08±1.26	0.21±0.27	0.19±0.18	0.40	0.27±0.29	42	44±18
	±2.1	±2.25					±0.42		±12	
clean	0.48±2	1.61±1.1	0.27±0.34	0.69±0.55	0.04±0.02	0.24±0.15	0.05	0.27±0.22	42	43±17
							±0.07		±29	
all	1.22	1.62±1.9	0.71±0.93	0.92±1.06	0.13±0.22	0.21±0.17	0.22	0.28±0.26	43	46±18
	±3.2						±0.35		±22	

6

7

8

9

10

11

12

13

14

15

16

17

18

19

20

21

22

23

24

25

26

1 Table 5. Summary of the different periods during the cloud event observed in 22-24  
 2 October 2011.

3

	period	time	sector	Temperature (C°)	special characteristics
1	rainy	22 October 9:00-12:00	polluted	0.9	rainy
2	clean	22-23 October 22:00-5:45	clean	-0.3	none
3	paper mill	23 October 5:45-6:15	1	-0.6	paper mill plume
4	clean 2	23 October 6:40-8:50	clean, 1	-0.7	none
5	heating plant	23 October 9:45-13:00	polluted	-0.5	heating plant plume
6	southern 1	23 October 14:00-15:45	polluted	0	none
7	southern 2	23 October 17:45-23:05	polluted	1.6	none
8	southern 3	23-24 October 23:05-5:15	polluted	3.6	none

4

5

6

7

8

9

10

11

12

13

14

15

16

17

18

19

20

21

22

23

1 Table 6. Average values and standard deviations of total particle number concentration  
 2 ( $N_{\text{tot}}$ ), geometric mean particle diameter (GMD), accumulation mode particle number  
 3 concentration ( $N_{\text{acc}}$ ), diameter of 50 % activation ( $D_{50}$ ), cloud droplet number  
 4 concentration ( $N_d$ ), droplet diameter ( $D_d$ ) and liquid water content (LWC) for the  
 5 different periods of the cloud event observed on 22-24 October 2011.

6

period	$N_{\text{tot}}$ (cm <sup>-3</sup> )	GMD (nm)	$N_{\text{acc}}$ (cm <sup>-3</sup> )	$D_{50}$ (nm)	$N_d$ (cm <sup>-3</sup> )	$D_d$ (μm)	LWC (g m <sup>-3</sup> )
rainy	2200±576	35±3	149±37	119±9	219±69	9.2±1.1	0.11±0.04
clean	451±195	49±8	62±18	112±20	138±32	12.2±1.9	0.17±0.08
paper mill	357±74	82±11	139±44	202±106	240±53	10.9±0.8	0.22±0.04
clean 2	214±22	77±5	83±9	146±28	152±30	11.8±0.6	0.16±0.04
heating plant*	1130±499	35±9	169±50	273±89	-	-	-
southern 1*	987±199	29±7	114±19	118±17	-	-	-
southern 2	801±388	40±10	123±26	118±30	234±49	10.0±1.0	0.15±0.04
southern 3	754±135	59±7	169±41	163±20	197±50	12.4±1.7	0.30±0.09

7

8 \*Cloud droplet probe frozen during these periods, data missing or otherwise unreliable.

9

10

11

12

13

14

15

16

17

18

19

20

21

22

23

24

1 Table 7. Average mass concentrations and standard deviations from the total line,  
 2 activated concentration (difference in the mass concentration between total and interstitial  
 3 lines) and activated fraction of chemical constituents for the different periods of the cloud  
 4 event observed on 22-24 October 2011.

5

period	Organics			SO <sub>4</sub> (μg m <sup>-3</sup> )			NO <sub>3</sub> (μg m <sup>-3</sup> )			NH <sub>4</sub> (μg m <sup>-3</sup> )			inorg.
	tot (μg m <sup>-3</sup> )	act (μg m <sup>-3</sup> )	act frac (%)	tot (μg m <sup>-3</sup> )	act (μg m <sup>-3</sup> )	act frac (%)	tot (μg m <sup>-3</sup> )	act (μg m <sup>-3</sup> )	act frac (%)	tot (μg m <sup>-3</sup> )	act (μg m <sup>-3</sup> )	act frac (%)	/total (%)
rainy	0.72	0.45	62	0.16	0.13	78	0.15	0.12	79±1	0.05	0.05	94	34
	±0.22	±0.26	±22	±0.06	±0.07	±14	±0.05	±0.05	1	±0.03	±0.03	±9	±7
clean	0.42	0.29	71	0.20	0.18	91	0.23	0.21	91	0.10	0.10	98	59
	±0.28	±0.34	±52	±0.15	±0.15	±15	±0.05	±0.05	±7	±0.05	±0.05	±6	±14
paper mill	0.69	0.58	84	2.46	2.2	90	0.42	0.35	85	0.99	0.90	91	85
	±0.16	±0.2	±17	±0.86	±0.90	±12	±0.01	±0.07	±16	±0.31	±0.33	±12	±2
clean 2	0.61	0.50	82	0.57	0.49	86	0.27	0.24	88	0.24	0.23	95	64
	±0.12	±0.22	±30	±0.08	±0.09	±08	±0.04	±0.04	±5	±0.04	±0.04	±4	±4
heating plant	0.69	0.56	80	4.43	3.4	77	0.08	0.06	78	0.52	0.46	87	87±7
	±0.30	±0.34	±26	±1.62	±1.81	±20	±0.08	±0.08	±29	±0.34	±0.36	±23	
southern 1	0.72	0.57	80	0.47	0.44	95	0.14	0.13	89	0.13	0.13	99	51
	±0.17	±0.29	±34	±0.19	±0.19	±7	±0.03	±0.03	±5	±0.05	±0.05	±1	±9
southern 2	0.81	0.66	82	0.66	0.62	93	0.15	0.13	89	0.16	0.16	99	54
	±0.23	±0.30	±25	±0.28	±0.29	±8	±0.07	±0.07	±7	±0.06	±0.06	±2	±8
southern 3	1.28	0.83	65	0.46	0.37	81	0.17	0.13	79	0.12	0.11	94	38±6
	±0.36	±0.43	±21	±0.25	±0.26	±19	±0.08	±0.08	±17	±0.10	±0.11	±21	

6

7

8

9

10

11

12

13

14

15

16

17

18

19

1 Table 8. Average values and standard deviations of particle hygroscopic growth factors  
 2  $GF_H$  and the ratios between more and less hygroscopic particle number concentrations,  
 3  $R_{GF} = N_{GF>1.25} / N_{GF\leq 1.25}$  for the different periods of the cloud event observed on 22-24  
 4 October 2011.

5

period	80 nm		100 nm		150 nm	
	$GF_H$	$R_{GF}$	$GF_H$	$R_{GF}$	$GF_H$	$R_{GF}$
rainy	1.16±0.04	0.42±0.12	1.25±0.04	1.43±0.45	1.33±0.02	2.69±0.63
clean	1.24±0.05	0.79±0.39	1.42±0.08	4.90±2.47	1.55±0.08	26.0±16.4
paper mill	1.17±0.02	0.44±0.07	1.37±0.01	2.06±0.34	1.56±0.06	23.9±10.9
clean 2	1.28±0.04	1.29±0.44	1.45±0.03	9.13±4.29	1.53±0.02	5.15±1.56
heating plant	1.24±0.11	1.09±1.02	1.36±0.09	3.74±3.79	1.48±0.03	8.75±6.83
southern 1	1.22±0.05	0.92±0.41	1.32±0.12	3.73±3.84	1.39±0.03	12.8±8.93
southern 2	1.20±0.06	0.62±0.31	1.34±0.07	2.50±1.29	1.43±0.04	3.03±1.18
southern 3	1.17±0.03	0.36±0.15	1.21±0.03	0.88±0.32	1.34±0.05	7.64±2.78
rainy	1.16±0.04	0.42±0.12	1.25±0.04	1.43±0.45	1.33±0.02	2.69±0.63

6

7

8

9

10

11

12

13

14

15

16

17

18

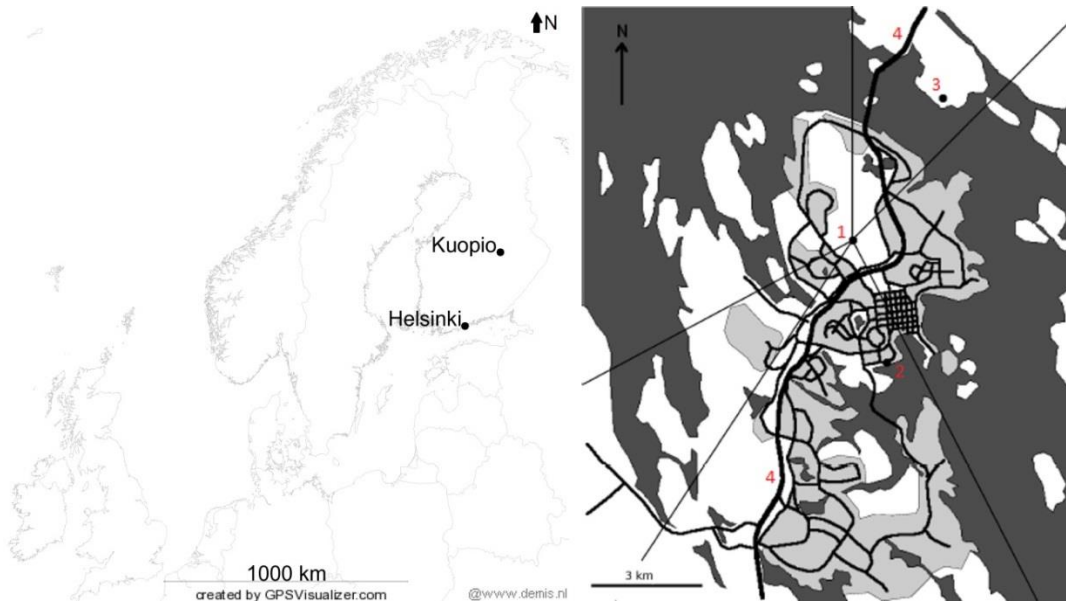
19

20

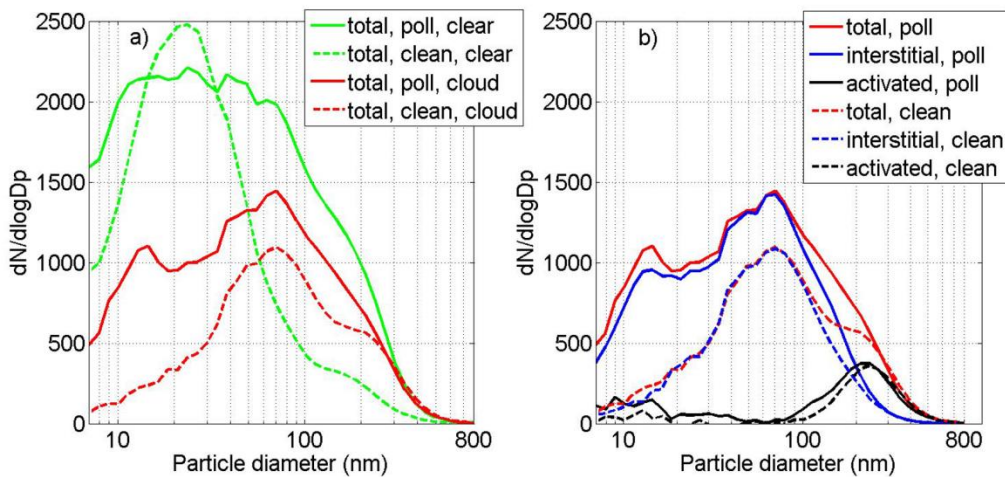
21

22

23

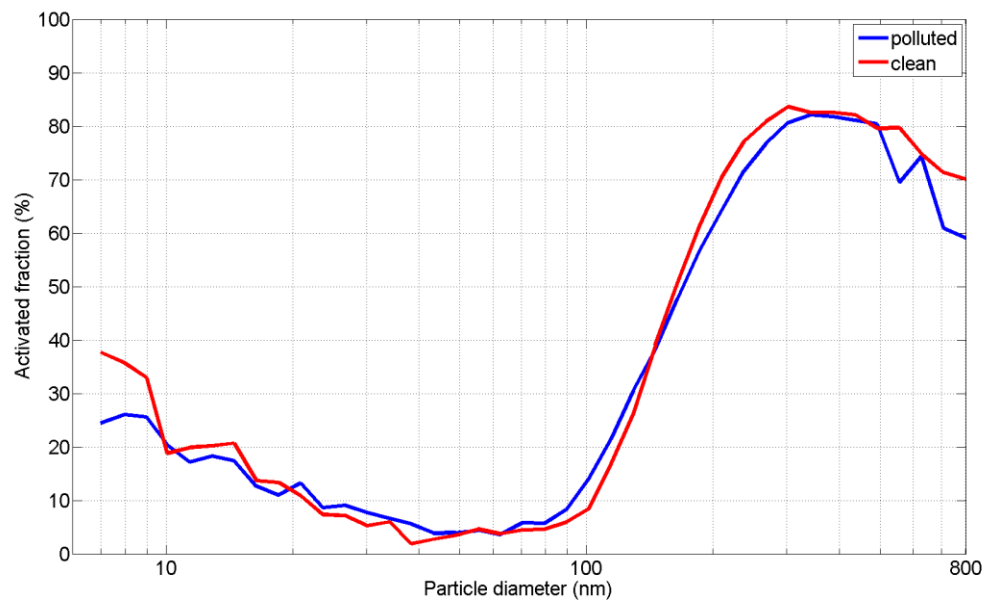


1  
 2 Figure 1. The location of Kuopio (left) and the map of the Kuopio area (right). Marked in  
 3 the Kuopio area map are Puijo (1), a heating plant (6), a paper mill (7) and a highway (8).  
 4 Dark grey color presents lakes, light grey residential areas and white forests. Also shown  
 5 are the five sectors used in the data analysis to distinguish the effect of local sources  
 6 (described in Sect. 2.4).



8  
 9  
 10 Figure 2. a) Average total particle size distributions in both clear and cloudy conditions  
 11 and b) average total, interstitial, and activated particle size distributions for polluted and  
 12 clean sectors in cloudy conditions.

13



1

2 Figure 3. Average activated fractions as a function of particle diameter for polluted and  
 3 clean sectors.

4

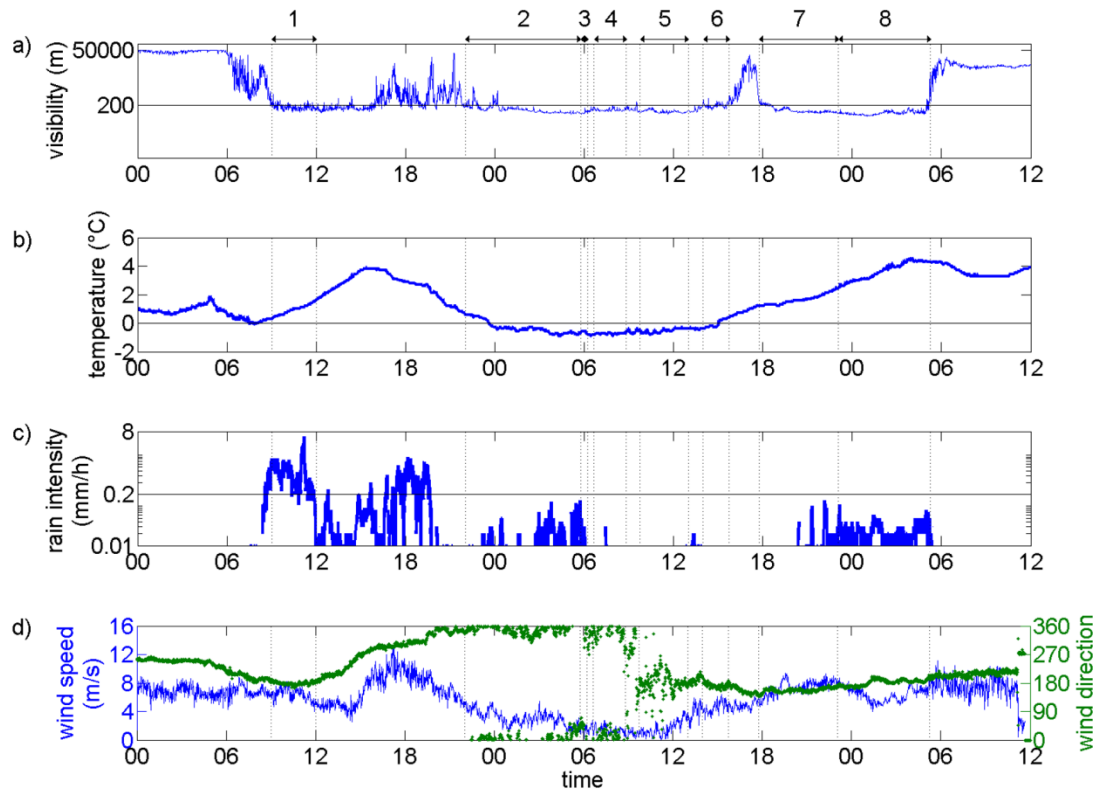
5

6

7

8





1

2 Figure 4. Time series of weather parameters observed during the cloud event on 22-24  
 3 October 2011. a) visibility, b) temperature, c) rain intensity, d) wind speed (left axis) and  
 4 direction (right axis). Different periods described in the text are marked with dashed lines  
 5 and also with numbered arrows above a) (1 = rainy, 2 = clean, 3 = paper mill, 4 = clean 2,  
 6 5 = heating plant, 6 = southern 1, 7 = southern 2, 8 = southern 3).

7

8

9

10

11

12

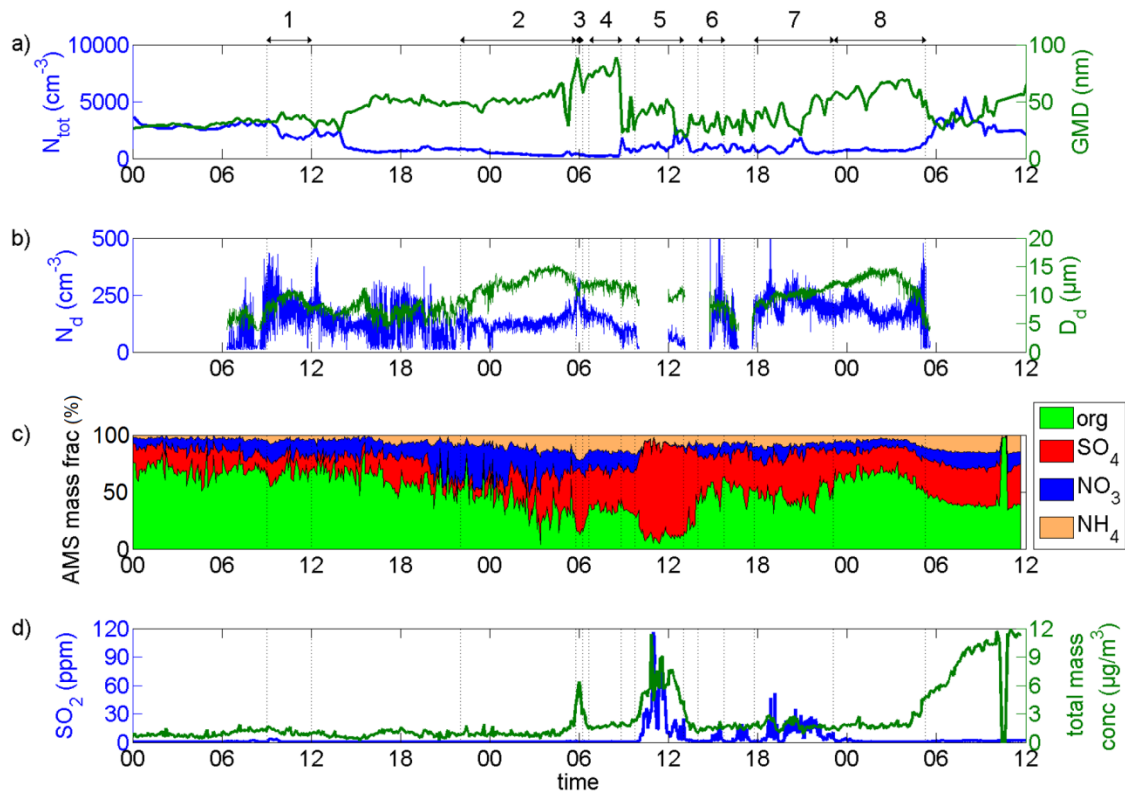
13

14

15

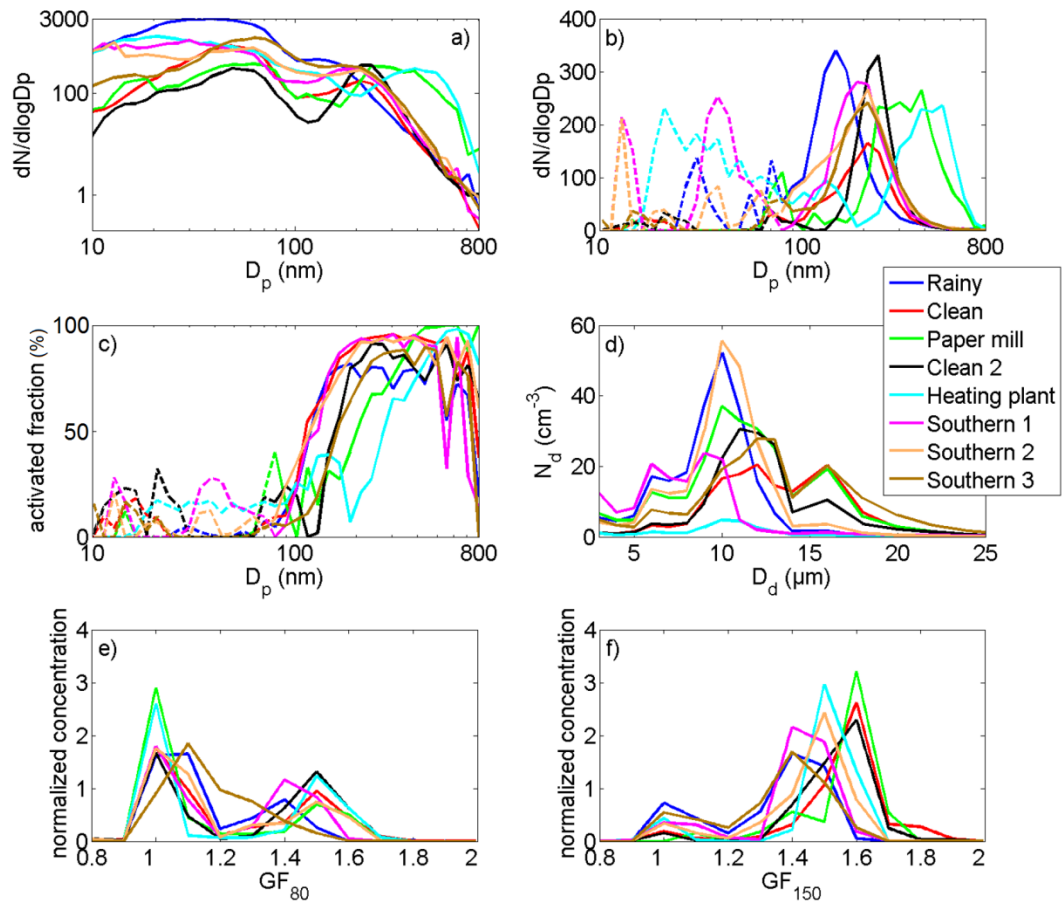
16

17



1  
2  
3  
4  
5  
6  
7  
8  
9  
10  
11  
12  
13  
14  
15  
16  
17

Figure 5. Time series during the cloud event on 22-24 October 2011 of a) total particle number concentration (left axis) and geometric mean particle diameter (right axis), b) cloud droplet number concentration (left axis) and mean droplet diameter (right axis), c) mass fractions of different chemical components measured by the AMS and d)  $\text{SO}_2$  concentration (left axis) and total particle mass concentration measured by the AMS (right axis). Different periods described in the text are marked with dashed lines and also with numbered arrows above a) (1 = rainy, 2 = clean, 3 = paper mill, 4 = clean 2, 5 = heating plant, 6 = southern 1, 7 = southern 2, 8 = southern 3).



1

2 Figure 6. a) Total particle size distributions, b) size distributions of activated particles, c)   
 3 activated fraction of particles as a function of particle diameter, d) cloud droplet size   
 4 distributions and growth factor distributions for e) 80 nm and f) 150 nm particles for the   
 5 different periods of the cloud event observed on 22-24 October 2011. In b) and c) data for   
 6 particles smaller than 80 nm in diameter are illustrated with dashed lines due to the   
 7 inaccuracies discussed in the text. In e) and f) normalized concentration means that the   
 8 integral of the particle concentrations over GF equals 100.

9

10

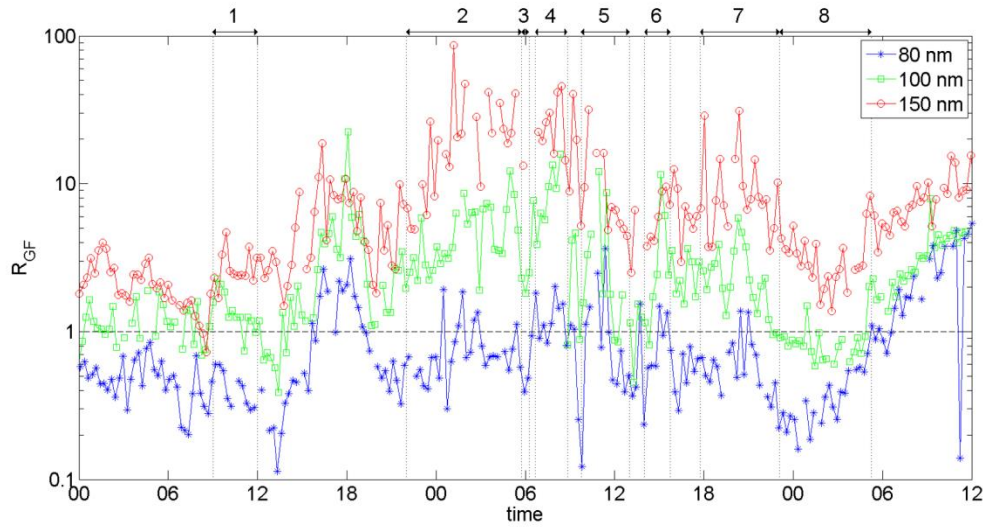
11

12

13

14

15



1  
 2 Figure 7. Time series of the ratio between the number concentrations of more and less  
 3 hygroscopic particles,  $R_{GF} = N_{GF>1.25}/N_{GF\leq 1.25}$  observed during the cloud event on 22-24  
 4 October 2011. Different periods described in the text are marked with dashed lines and  
 5 also with numbered arrows (1 = rainy, 2 = clean, 3 = paper mill, 4 = clean 2, 5 = heating  
 6 plant, 6 = southern 1, 7 = southern 2, 8 = southern 3).